MOLECULAR AND CELLULAR BIOLOGY
2023, VOL. 43, NO. 7, 301–316
https://doi.org/10.1080/10985549.2023.2210030

Taylor & Francis
Taylor & Francis Group

RESEARCH ARTICLE

microRNA-130b May Induce Cerebral Vasospasm after Subarachnoid Hemorrhage via Modulating Kruppel-like Factor 4

Zewei Huang, Jiliang Hu, Jiongfu Xu, Hao Wang, Limeng Dai

[a]Department of Critical Care Medicine, Shenzhen People's Hospital (The Second Clinical Medical College, Jinan University; The First Affiliated Hospital, Southern University of Science and Technology), Shenzhen, P. R. China

[b]Department of Neurosurgery, Shenzhen People's Hospital (The Second Clinical Medical College of Jinan University; The First Affiliated Hospital of Southern University of Science and Technology), Shenzhen, P. R. China

[c]Guangdong Engineering Technological Research Center for nervous anatomy and Related Clinical Applications, Shenzhen, P. R. China

ABSTRACT Recently, the diverse functions of microRNAs (miRNAs) in brain diseases have been demonstrated. We intended to uncover the functional role of microRNA-130b (miR-130b) in cerebral vasospasm (CVS) following subarachnoid hemorrhage (SAH). SAH was induced by injecting the autologous blood into the cisterna magna of Sprague Dawley rats. The cerebral vascular smooth muscle cells (cVSMCs) were extracted for in vitro experimentation. In vitro and in vivo assays were implemented with transfection of miR-130b mimic/inhibitor, sh-Kruppel-like factor 4 (*KLF4*), oe-*KLF4* plasmids or p38/MAPK signaling pathway agonist (anisomycin), respectively, to elaborate the role of miR-130b in CVS following SAH. Elevated miR-130b and reduced *KLF4* were found in SAH patients and rat models of SAH. *KLF4* was the target gene of miR-130b. miR-130b promoted the proliferation and migration of cVSMCs through the Inhibition of *KLF4*. Besides, *KLF4* inhibited the proliferation and migration of cVSMCs through blockage of the p38/MAPK pathway. Furthermore, in vivo assay confirmed the inhibitory effect of decreased miR-130b in CVS following SAH. In conclusion, miR-130b may activate the p38/MAPK signaling pathway through targeted inhibition of *KLF4*, thereby contributing to some extent to the development of cerebral vasospasm after SAH.

KEYWORDS microRNA-130b, cerebral vasospasm, subarachnoid hemorrhage, KLF4, p38/MAPK signaling pathway

INTRODUCTION

Subarachnoid hemorrhage (SAH), a well-known neurologic emergency, is bleeding in the subarachnoid space between the arachnoid and pia mater.[1] Empirical evidence has shown that the overall incidence rate of SAH is 9 per 100,000, and up to 40% of patients are likely to die of SAH, whereas 50–66% will suffer permanent disability.[2] The main symptom of SAH is characterized as a sudden and severe headache classically described as the "worst headache of life" combined with a brief loss of consciousness, nausea or vomiting, meningism, and seizures.[3] Patients suffering from SAH may also exhibit various complications, including rebleeding, cerebral edema, cerebral vasospasm (CVS), and cerebral ischemia.[4] Although the risk factors for SAH are highly uncertain due to its low incidence, the most common risk factors include female gender, hypertension, smoking, and the prevalence and growth of intracranial aneurysms.[5] Although the morbidity and mortality rate of SAH has declined over the past few decades, the further progress of SAH clinical treatment is slow, and many randomized clinical trials have failed to improve the prognosis of patients.[6]microRNAs (miRNAs) are highly tissue-specific elements that not only play an intracellular role but

Address correspondence to Hao Wang, wang.hao1@szhospital.com; dai.limeng@szhospital.com

The authors declare no conflict of interest.

Received 24 February 2022
Revised 17 April 2023
Accepted 17 April 2023

also remain functional while delivered outside the cells in exosomes and exist stably in body fluids.[7] Dysregulated expression of miRNAs has been found to correlate with cancer-related diseases, cardiovascular diseases, and some neurological conditions.[8–10] Interestingly, SAH has also been attributed to the significant changes in the miRNA profile.[11,12] miR-130b plays a key regulatory role in glioma, diabetic encephalopathy, and acute spinal cord injury via cell proliferation, apoptosis, invasion, and migration.[13–15] Furthermore, highly expressed miR-130b has been found in multiple cancers, and overexpression of miR-130b could enhance cancer cells' proliferation and invasion ability.[16,17] Specifically, miR-130b is oncogenic in lung cancer by targeting *PTEN*.[18] Furthermore, another study has demonstrated that miR-130b-5p may be an appealing target for coronary artery disease.[19] Interestingly, the roles of miR-130b in cerebral ischemia/reperfusion injury have been reported,[20,21] while the effects of miR-130b on CVS after SAH remain to be further elucidated.

In the present study, we predicted that miR-130b could target Kruppel-like factor 4 (*KLF4*). *KLF4* is a zinc-finger transcription factor of the Kruppel-like factor family with the ability to regulate different vascular functions, such as vascular tone and permeability, as well as angiogenesis.[22–24] Previous evidence has reported the decreased expression of *KLF4* mRNA in the cerebrospinal fluid (CSF) and plasma of patients with SAH.[25] Considering these findings, we predicted that miR-130b and *KLF4* might play important roles in CVS after SAH. Here we aimed to decipher the underlying mechanisms concerning miR-130b in CVS after SAH by targeting *KLF4*.

RESULTS

Highly expressed miR-130b and lowly expressed *KLF4* in SAH patients. Following the collection of CSF, expression of miR-130b and *KLF4* was detected by RT-qPCR. Our results depicted that the expression of miR-130b in SAH patients was significantly increased, reaching the highest level on day 1. Still, it gradually decreased over time and remained higher than the controls. In contrast, *KLF4* expression in the CSF of SAH patients was significantly decreased, which was the lowest on day 1, but gradually increased over time and remained lower than the controls (Fig. 1A). Consistently, ELISA results also confirmed the reduced *KLF4* expression in the CSF of SAH patients (Fig. 1B).

These results indicated that miR-130b was highly expressed, and *KLF4* was lowly expressed in patients with CVS after SAH relative to the controls.

Highly expressed miR-130b and lowly expressed *KLF4* in rat models of CVS after SAH. Neurobehavioral scores were obtained at 12, 24, 48, and 72 h after modeling. The result demonstrated that SAH rats showed increased neurobehavioral scores and behavioral disorders, while neurobehavioral scores were highest and the behavioral disorders were the most serious at 24 h after model establishment (Fig. 2A). The CSF and basilar arteries of the two groups of rats were collected at 12, 24, 48, and 72 h after modeling. The basilar arteries were embedded, and the vasospasm was observed by H&E staining. We found that SAH rats showed serious vasospasm while the most

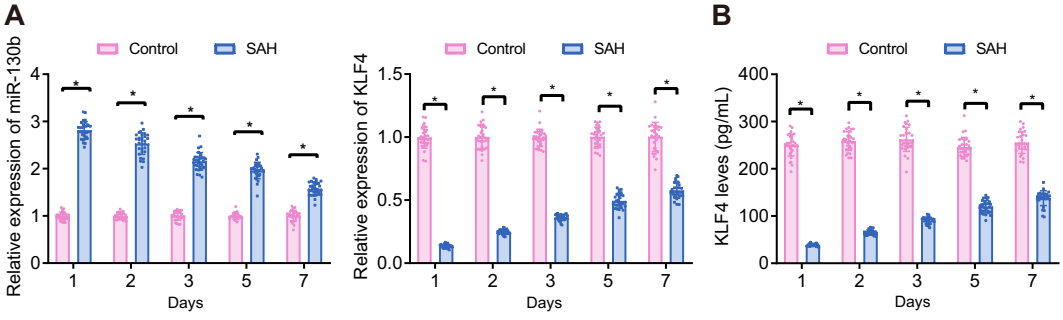

FIG 1 miR-130b was highly expressed, and *KLF4* was lowly expressed in patients with CVS after SAH. (A) Expression of miR-130b and *KLF4* in CSF of healthy patients ($n = 30$) and SAH patients ($n = 30$) detected by RT-qPCR. (B) *KLF4* expression in CSF of healthy patients ($n = 30$) and SAH patients ($n = 30$) measured by ELISA. $^*P < 0.05$. Comparison of data between groups at different time points was conducted by repeated measures analysis of variance, followed by Bonferroni correction.

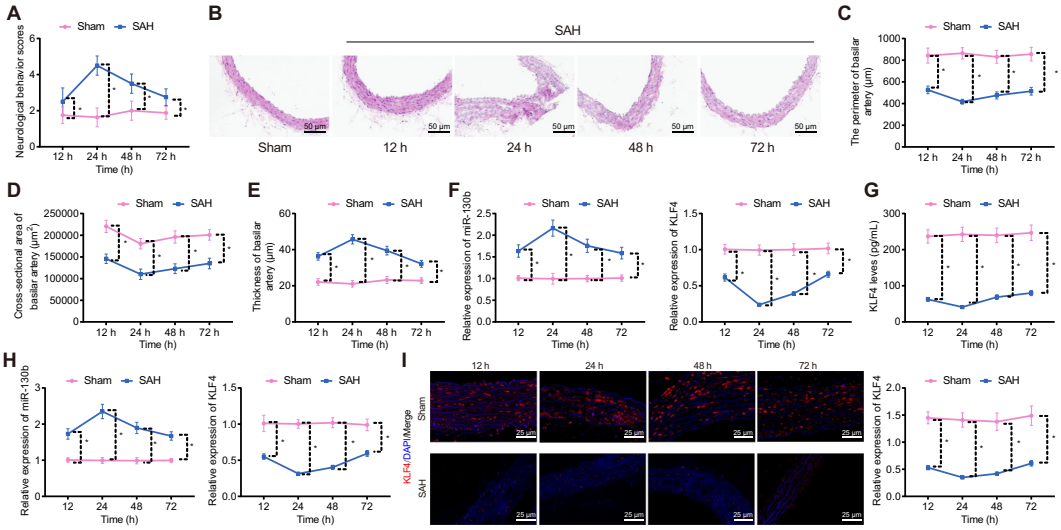

FIG 2 Highly expressed miR-130b and lowly expressed *KLF4* in rat models of SAH. (A) Neurologic deficit scores at 12, 24, 48 and 72 h after modeling. (B) HE staining for the cross section of the basilar artery of SAH rats (scale bar: 50 μm). (C to E) The semi-quantitative analysis of perimeters of the vascular ring (C), vascular lumen area (D), vascular wall thickness (E) of the cerebral basilar artery in SAH rats by H&E staining. (F) Expression of miR-130b and *KLF4* in CSF in SAH rats detected by RT-qPCR. (G) *KLF4* expression in CSF in SAH rats measured by ELISA; (H) Expression of miR-130b and *KLF4* in the basilar artery in SAH rats detected by RT-qPCR; I, *KLF4* expression in the basilar artery in SAH rats detected by immunofluorescence staining (scale bar: 25 μm). $^{*}P < 0.05$. Data between the two groups were compared by paired *t* test. In comparisons among more than two groups, a one-way analysis of variance was used, followed by Tukey's post hoc test. Comparison of data between groups at different time points was conducted by repeated measures analysis of variance followed by Bonferroni correction.

serious vasospasm was observed at 24 h (Fig. 2B). In addition, the perimeter of blood vessels and lumen area of blood vessels were significantly reduced, and the vascular walls were significantly thickened in SAH rats. At 24 h, the perimeter and lumen area of blood vessels was the lowest, and the vascular wall was the thickest (Fig. 2C to E).

Our results from RT-qPCR revealed that the expression of miR-130b in CSF and basilar artery in SAH rats was significantly increased with the highest expression on day 1 but then gradually decreased over time and remained higher than the sham-operated rats, while the mRNA level of *KLF4* in CSF and basilar artery in SAH rats was significantly decreased with the lowest on day 1, but then gradually increased over time, and remained lower than the sham-operated rats (Fig. 2F and H). The ELISA results also confirmed the low mRNA level of *KLF4* in the CSF of SAH rats (Fig. 2G). Immunofluorescence results also verified the changes in protein expression of *KLF4* in the basilar artery in SAH rats at 12, 24, 48, and 72 h after modeling. In addition, *KLF4* protein was expressed in the nucleus and cytoplasm (Fig. 2I).

Thus, miR-130b was highly expressed, and *KLF4* was lowly expressed in the rat model of CVS following SAH relative to the sham-operated rats.

***KLF4* is the target gene of miR-130b.** Venn diagram analysis of the target genes of miR-130b predicted by the StarBase, RNAInter, RNA22, miRanda, and mirDIP databases revealed nine candidate genes, i.e., *KLF4*, *STX6*, *IRF1*, *IGF1*, *UXS1*, *BTG1*, *RPA2*, *SYT1*, and *TP63* (Fig. 3A). The potential negative correlation of miR-130b expression with *KLF4* expression was verified in clinical samples and animal experiments. To further detect their correlation, the TargetScan website was used, which predicted miR-130b binding sites in *KLF4* 3'UTR in humans (Fig. 3B). The luciferase reporter assay was used to verify that *KLF4* was the target of miR-130b in cVSMCs. Our experimental results showed that miR-130b mimic exhibited no significant effects on the luciferase activity of the *KLF4*-MUT while reducing that of *KLF4*-WT. In addition, the miR-130b inhibitor increased the luciferase activity of the *KLF4*-WT while failing to affect that of *KLF4*-MUT (Fig. 3C), suggesting that miR-130b could specifically bind to *KLF4*.

RT-qPCR and Western blot analysis verified that miR-130b expression was increased and *KLF4* expression was decreased in cVSMCs transduced with miR-130b mimic,

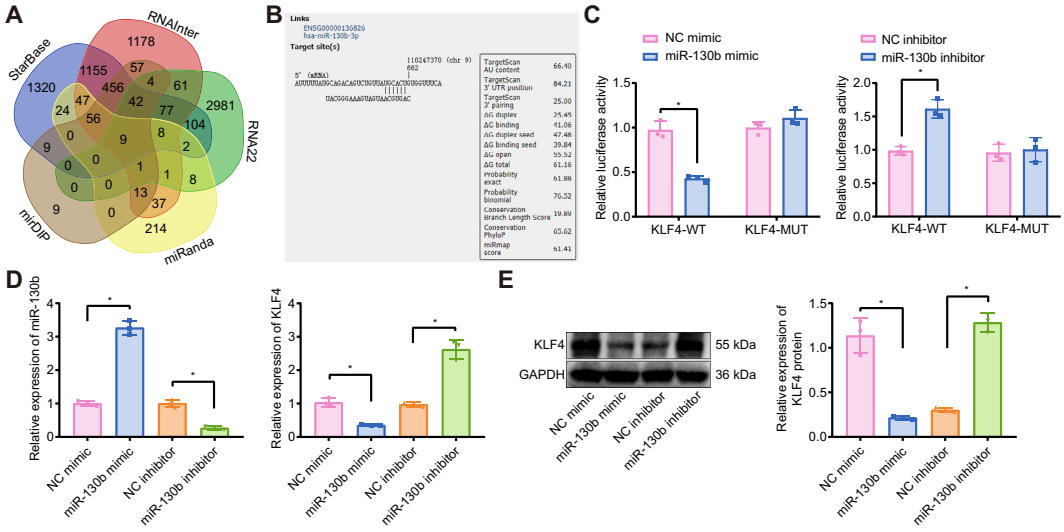

FIG 3 miR-130b targets *KLF4*. (A) Venn diagram analysis of the target genes of miR-130b predicted by the StarBase, RNAInter, RNA22, miRanda, and mirDIP databases. (B) The binding site between miR-130b and *KLF4* predicted by the TargetScan database. (C) The target relationship between miR-130b and *KLF4* demonstrated by dual luciferase reporter assay in sVSMCs. (D) Expression of miR-130b and *KLF4* in cVSMCs transduced with miR-130b mimic or miR-130b inhibitor detected by RT-qPCR. (E) Expression of *KLF4* in cVSMCs transduced with miR-130b mimic or miR-130b inhibitor measured by Western blot analysis. $^{*}P < 0.05$. The cell experiment was run in triplicate independently. Data between the two groups were compared by paired *t* test. In comparisons among more than two groups, a one-way analysis of variance was used, followed by Tukey's post-hoc test.

while the results were opposite in cVSMCs transduced with miR-130b inhibitor (Fig. 3D and E).

Our results elaborated that miR-130b could target *KLF4*.

miR-130b may promote the proliferation and migration of cVSMCs through the inhibition of *KLF4*. Previous studies have reported that VSMC phenotypic switching was engaged in vascular remodeling and was correlated with neurological deficits after SAH.[26] Thus, here we further investigated these findings at the cellular level. cVSMCs were isolated from SD rats. The VSMC marker protein α-SMA was labeled with immunofluorescence staining to identify the extracted primary cells as cVSMCs (Fig. 4A).

To verify the effects of miR-130b targeting *KLF4* on the proliferation and migration of cVSMCs, *KLF4* was downregulated in cVSMCs. RT-qPCR and Western blot analysis showed that mRNA and protein levels of *KLF4* were reduced in cVSMCs transduced with sh-*KLF4*-1 or sh-*KLF4*-2, with sh-*KLF4*-1 showing the superior silencing efficiency. Thus, sh-*KLF4*-1 was used for the subsequent experiments (Fig. 4B). Proliferation and migration of cVSMCs were induced by PDGF-BB (20 ng/mL). After PDGF-BB intervention for 24 h, cVSMCs were transduced with miR-130b inhibitor or sh-*KLF4*. As described by RT-qPCR and Western blot analysis, PDGF-BB intervention increased miR-130b expression and decreased the mRNA and protein levels of *KLF4* in cVSMCs. Moreover, miR-130b expression was reduced, and the mRNA and protein levels of *KLF4* were elevated in cVSMCs treated with PDGF-BB + miR-130b inhibitor, while miR-130b expression showed no obvious difference, and the mRNA and protein levels of *KLF4* were reduced in cVSMCs treated with PDGF-BB + sh-*KLF4*. Besides, compared with cVSMCs treated with PDGF-BB + miR-130b inhibitor + sh-NC, miR-130b expression exhibited no significant difference, and the mRNA and protein levels of *KLF4* were decreased in cVSMCs treated with PDGF-BB + miR-130b inhibitor + sh-*KLF4* (Fig. 4C and D).

EdU and transwell assay illustrated that PDGF-BB intervention promoted proliferation and migration, while *KLF4* knockdown promoted the proliferation and migration of PDGF-BB-treated cVSMCs. Besides, the inhibitor of miR-130b suppressed the proliferation and migration of PDGF-BB-treated cVSMCs, while downregulation of both miR-130b and *KLF4* induced the proliferation and migration of PDGF-BB-treated cVSMCs (Fig. 4E and F and Fig. 5). Furthermore, proliferation-related (PCNA) and migration-related proteins (MMP2, MMP3, and MMP9) were determined, and the results

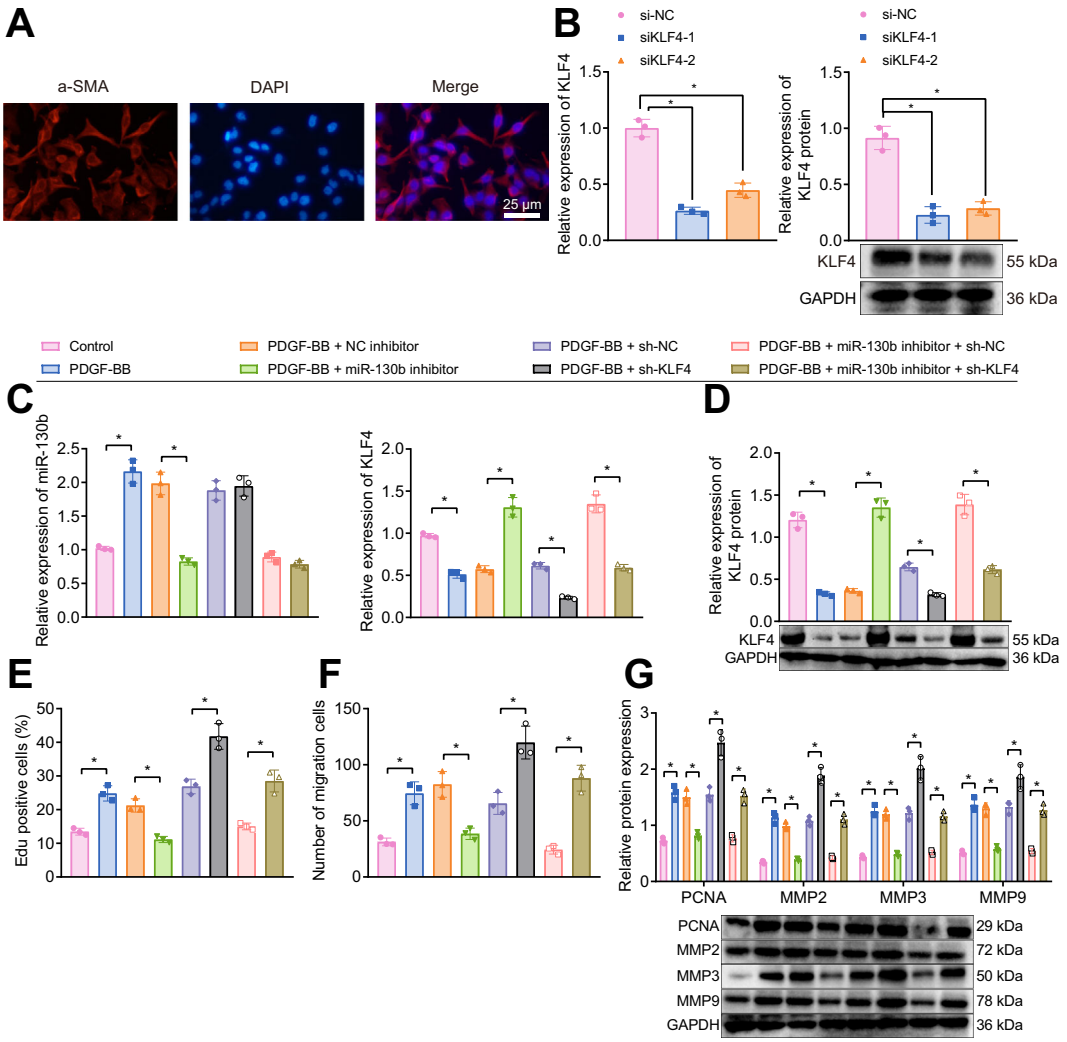

FIG 4 miR-130b enhances the proliferation and migration of cVSMCs through the downregulation of *KLF4*. (A) The VSMC marker protein α-SMA labeled with immunofluorescence staining to identify the cVSMCs. (B) Silencing effect of *KLF4* in cVSMCs verified by RT-qPCR and Western blot analysis. cVSMCs were treated with PDGF-BB, miR-130b inhibitor, and/or sh-*KLF4*. (C) Expression of miR-130b and *KLF4* in cVSMCs detected by RT-qPCR. (D) Expression of *KLF4* in cVSMCs measured by Western blot analysis. (E) Proliferation of cVSMCs detected by EdU assay. (F) Migration of cVSMCs detected by transwell assay. (G) Expression of p38/MAPK signaling pathway-related proteins, PCNA, MMP2, MMP3, and MMP9 in cVSMCs detected by Western blot analysis. $^*P < 0.05$. The cell experiment was run in triplicate independently. Data between the two groups were compared by paired *t* test. The one-way analysis of variance was used for comparisons among more than two groups, followed by Tukey's post hoc test.

demonstrated that PDGF-BB intervention elevated the expression of PCNA, MMP2, MMP3, and MMP9 in cVSMCs, and further *KLF4* knockdown also increased the expression of PCNA, MMP2, MMP3, and MMP9 in PDGF-BB-treated cells. Moreover, downregulation of miR-130b reduced PCNA, MMP2, MMP3, and MMP9 in PDGF-BB-treated cVSMCs, while both silenced of miR-130b and *KLF4* elevated expression of PCNA, MMP2, MMP3, and MMP9 (Fig. 4G).

These results suggested that miR-130b may promote the proliferation and migration of cVSMCs by inhibiting *KLF4*.

***KLF4* could repress proliferation and migration of cVSMCs through blockage of the p38/MAPK signaling pathway.** hTFtarget was used to predict the target gene of *KLF4*, while protein-protein interaction (PPI) analysis of the target genes was performed by STRING. The minimum required interaction score >0.9 was set, and the visualization results of PPI analysis were obtained through the Cytoscape software (Fig. 6A). We found that the three genes, *CDC42*, *RHOA*, and *MAPK1*, were in the core position of the network map and exhibited degree >30 (Fig. 6B). Moreover, it has been reported that

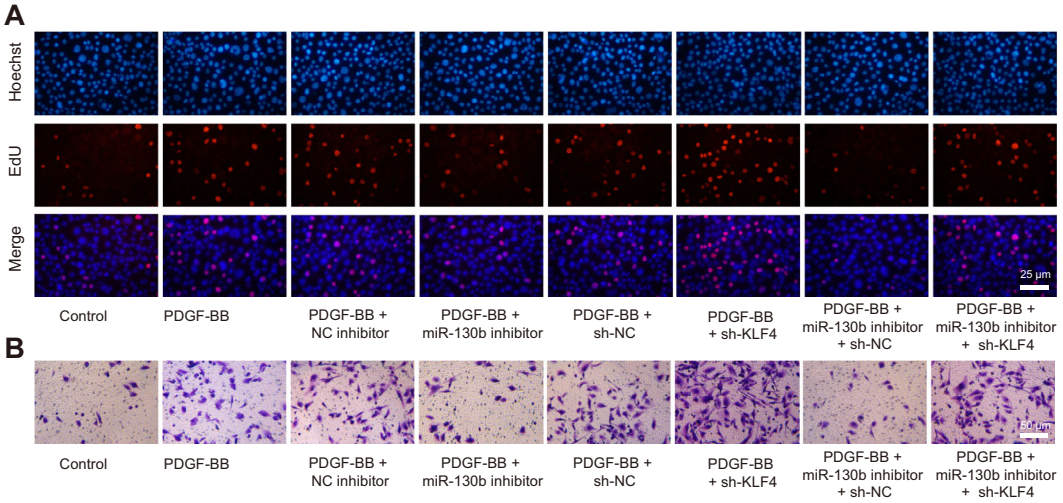

FIG 5 Cell proliferation and migration in different groups. (A) Representative images of the proliferation of cVSMCs detected by transwell assay in Fig. 4E (scale bar: 25 μm). (B) Representative images of migration of cVSMCs detected by transwell assay in Fig. 4F (scale bar: 50 μm).

KLF4 can negatively regulate the p38/MAPK signaling pathway.[27] While activation of the p38/MAPK signaling pathway induces the occurrence of SAH[28] along with the proliferation and migration of VSMCs.[29] Intriguingly, our results indicated a targeting relationship between *KLF4* and *p38* (*MAPK1*) through hTFtarget search (Fig. 6C). To further assay the relationship between *KLF4* and *p38*, we predicted the binding of *KLF4* and p38 through the JASPAR (Fig. 6D and Fig. 7).

To investigate whether *KLF4* could inhibit the proliferation and migration of VSMCs by inhibiting the activation of the p38/MAPK signaling pathway, oe-NC, and oe-*KLF4* plasmids were transfected into cVSMCs, respectively. The results of RT-qPCR and Western blot analysis showed that compared with the oe-NC group, the expression of *KLF4* mRNA and protein was significantly increased in the oe-*KLF4* group (Fig. 6E). In addition, no significant change was found in p38 expression in cVSMCs following each treatment. PDGF-BB intervention increased the expression of PCNA, MMP2, MMP3, and MMP9 and the expression level of phosphorylated p38 while decreasing KLF4 expression. Upregulation of *KLF4* reversed these effects of PDGF-BB. Further treatment with anisomycin could also increase the expression of PCNA, MMP2, MMP3, and MMP9, as well as the expression level of phosphorylated p38 in cVSMCs, while *KLF4* displayed no evident difference (Fig. 6F). EdU and transwell assays manifested that PDGF-BB intervention promoted proliferation and migration of cVSMCs, whereas further upregulation of *KLF4* reversed the promotion in proliferation and migration caused by PDGF-BB intervention. Moreover, treatment with anisomycin and upregulation of *KLF4* could also promote the proliferation and migration of PDGF-BB-treated cVSMCs (Fig. 6G and H).

These results verified that *KLF4* repressed the proliferation and migration of cVSMCs through blockage of the p38/MAPK signaling pathway.

miR-130b could promote the proliferation and migration of cVSMCs by targeting *KLF4* via activation of the p38/MAPK signaling pathway. To further investigate the regulation of *KLF4* expression by miR-130b and its effects on the activation of the p38/MAPK signaling pathway, cVSMCs were pretreated with PDGF-BB for 24 h and then transduced with NC mimic, miR-130b mimic, oe-NC and oe-*KLF4*, and treated with anisomycin. RT-qPCR revealed that miR-130b expression was upregulated and *KLF4* expression was downregulated in cVSMCs transduced with miR-130b mimic. In contrast, miR-130b expression exhibited no obvious difference, and *KLF4* expression was elevated in cVSMCs transduced with miR-130b mimic and oe-*KLF4*. Further, anisomycin treatment did not affect the expression of miR-130b and *KLF4* (Fig. 8A). Western blot analysis indicated no significant change was found in p38 expression. Furthermore, upregulation of miR-130b increased the expression of PCNA, MMP2,

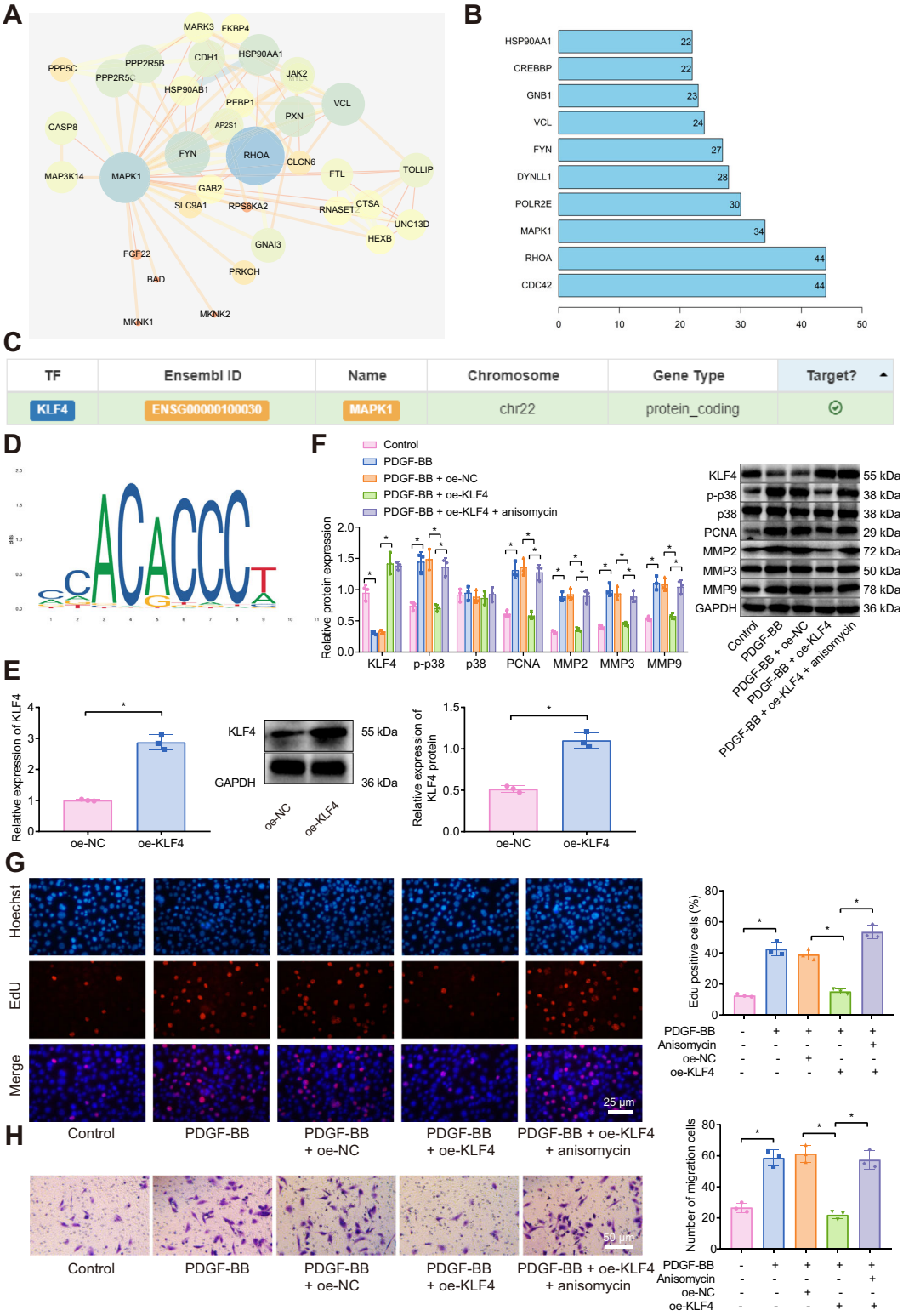

FIG 6 *KLF4* represses the proliferation and migration of cVSMCs through blockage of the p38/MAPK signaling pathway. (A) PPI network diagram of target genes of *KLF4*; The larger the circle, the higher the degree of the gene; The color of the circle from blue to orange indicates the degree value of the gene from large to small; The thicker the line between the circles, the stronger the link between the genes. (B) Bar chart of the number of associated genes which correlated with target genes; abscissa indicates degree value, ordinate indicates the name of genes. (C) Targeting relationship between *KLF4* and p38 (MAPK) confirmed by hTFtarget. (D) The binding site between *KLF4* and p38 (MAPK) predicted by JASPAR. (E) Overexpression effect of *KLF4* in cVSMCs verified by RT-qPCR and Western blot analysis. cVSMCs were treated with PDGF-BB, oe-*KLF4*, and/or anisomycin; (F) Expression of KLF4, the p38/MAPK signaling pathway-related proteins, PCNA, MMP2, MMP3, and MMP9 in cVSMCs detected by Western blot analysis. (G) Proliferation of cVSMCs detected by EdU assay. (H) Migration of cVSMCs detected by transwell assay. $^*P < 0.05$. The cell experiment was run in triplicate independently. Data between the two groups were compared by paired *t* test. One-way analysis of variance was used for the comparisons among more than two groups, followed by Tukey's post hoc test.

Matrix ID	Name	Score	Relative score	Sequence ID	Start	End	Strand	Predicted sequence
MA0039.1	MA0039.1.Klf4	8.64942	0.9107510648264169	MAPK1	994	1003	-	AAAAGACAGG
MA0039.1	MA0039.1.Klf4	7.7027965	0.8829637285695844	MAPK1	334	343	+	TACAAAAAGG
MA0039.3	MA0039.3.KLF4	9.965159	0.8793011752685437	MAPK1	1963	1973	+	GCACGCCCTTG
MA0039.1	MA0039.1.Klf4	7.42515	0.874813646477508	MAPK1	1392	1401	+	TAGAGCAAAG
MA0039.1	MA0039.1.Klf4	7.3929324	0.8738679286254726	MAPK1	950	959	-	AAATAAAAAG
MA0039.1	MA0039.1.Klf4	7.2569504	0.8698762896340686	MAPK1	1169	1178	+	ATAAGAAAAG
MA0039.1	MA0039.1.Klf4	7.202245	0.8682704659002601	MAPK1	944	953	-	AAAGCCAAGG
MA0039.1	MA0039.1.Klf4	7.065776	0.8642645218153198	MAPK1	1869	1878	-	CGGGGGAGGG
MA0039.1	MA0039.1.Klf4	7.01441	0.862756720165694	MAPK1	130	139	-	AAAAGCAGAG
MA0039.1	MA0039.1.Klf4	6.9483447	0.8608174281849101	MAPK1	793	802	-	AACTGAAAGG

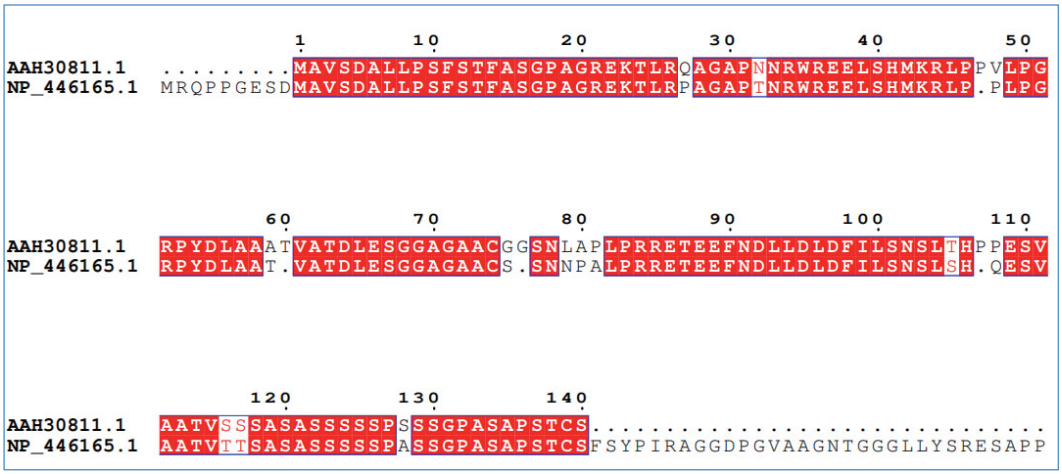

FIG 7 *KLF4* and MAPK1 binding potential in rats. (A) Rat MAPK1 promoter region (positions −2000 ~ 0) was imported into JASPAR for prediction of its transcription factor binding. (B) Comparison of human and rat *KLF4* conservatism.

MMP3, and MMP9, as well as the expression level of phosphorylated p38, while decreasing the expression of *KLF4*. At the same time, these changes were reversed by further overexpression of *KLF4*. Besides, anisomycin treatment in cells over-expressing miR-130b and *KLF4* showed increased expression of PCNA, MMP2, MMP3, and MMP9, as well as the expression level of phosphorylated p38. Still, no significant change was observed in *KLF4* expression (Fig. 8B). EdU and transwell assay demonstrated that overexpression of miR-130b promoted proliferation and migration, which were abolished by further upregulated *KLF4*. Moreover, anisomycin treatment in cells over-expressing miR-130b and *KLF4* enhanced proliferation and migration (Fig. 8C and D). These findings elicited that miR-130b could promote the proliferation and migration of cVSMCs by targeting *KLF4* to activate the p38/MAPK signaling pathway.

miR-130b could promote CVS following SAH by targeting *KLF4* via activation of the p38/MAPK signaling pathway in vivo. To further verify these above-reported findings, SAH rat models were then established. Inhibitor NC, miR-130b inhibitor, and anisomycin were injected into the brain of SD rats 24 h before modeling. Neurobehavioral scores were obtained at 24 h after modeling. Our result displayed that SAH rats showed increased neurobehavioral scores and behavioral disorders; rats with miR-130b inhibitor injection exhibited decreased neurobehavioral scores. However, these changes were reversed by the anisomycin injection (Fig. 9A). The CSF and basilar arteries of the two groups of rats were collected after 24 h of modeling. The basilar arteries were embedded, and the vasospasm was observed by HE staining. We found that SAH rats showed serious vasospasm, the reduced perimeter of the blood vessel and lumen area of blood vessels, as well as thickened vascular wall, whereas rats with miR-130b inhibitor injection manifested relieved vasospasm, the increased perimeter of blood vessels and lumen area of

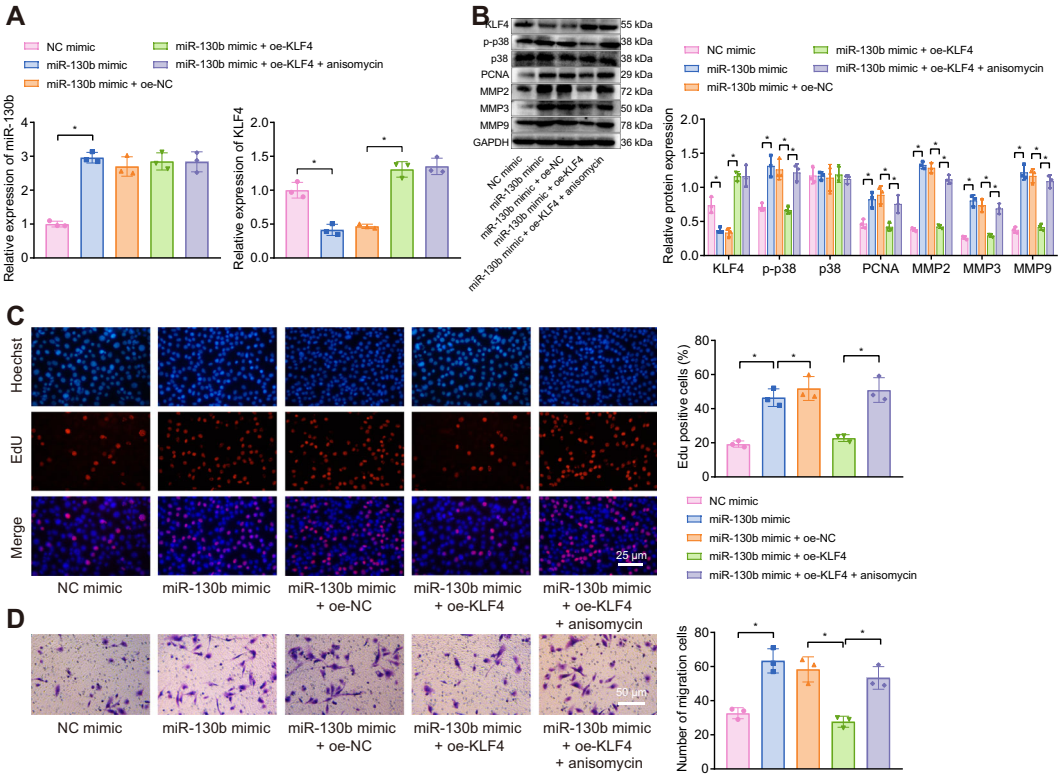

FIG 8 Upregulation of miR-130b enhances the proliferation and migration of cVSMCs by downregulating *KLF4* through activation of the p38/MAPK signaling pathway. cVSMCs were transduced with miR-130b mimic, oe-*KLF4*, and/or anisomycin. (A) expression of miR-130b and *KLF4* in cVSMCs detected by RT-qPCR. (B) Expression of p38/MAPK signaling pathway-related proteins, PCNA, MMP2, MMP3, and MMP9 in cVSMCs detected by Western blot analysis. (C) Proliferation of cVSMCs detected by EdU assay. (D) Migration of cVSMCs detected by transwell assay. $^*P < 0.05$. The cell experiment was run in triplicate independently. Data between the two groups were compared by paired *t* test. The one-way analysis of variance was used for comparisons among more than two groups, followed by Tukey's post hoc test.

blood vessels, as well as the thinned vascular wall. However, these changes were reversed by the anisomycin injection (Fig. 9B to E).

At 24 h after model establishment, CSF and basilar artery were isolated from SAH rats. Our results from RT-qPCR revealed that the expression of miR-130b in CSF and basilar artery in SAH rats was significantly increased, whereas the mRNA expression of *KLF4* in CSF and basilar artery in SAH rats was significantly decreased compared to sham-operated rats. Besides, miR-130b expression was decreased, and *KLF4* expression was increased in CSF of rats injected with miR-130b inhibitor, and further injection with anisomycin exerted no effects on expression of miR-130b and *KLF4* in CSF of rats injected with miR-130b inhibitor + anisomycin (Fig. 9F and H), which was confirmed by the ELISA results (Fig. 9G). Western blot analysis demonstrated that no significant change was found in p38 expression. SAH rats showed increased expression of PCNA, MMP2, MMP3, and MMP9, as well as the expression level of phosphorylated p38, while decreased *KLF4* expression was observed when compared with sham-operated rats. Downregulation of miR-130b significantly decreased the expression of PCNA, MMP2, MMP3, and MMP9, as well as the expression level of phosphorylated p38, while further anisomycin treatment increased the expression of PCNA, MMP2, MMP3, MMP9, as well as the expression level of phosphorylated p38, and no significant change was found in *KLF4* expression (Fig. 9I).

These results suggested that miR-130b could promote the CVS following SAH by targeting *KLF4* and activating the p38/MAPK signaling pathway.

DISCUSSION

Emerging evidence has highlighted a worldwide socioeconomic burden due to SAH; more than two-thirds of SAH patients suffer from cognitive impairment and poor

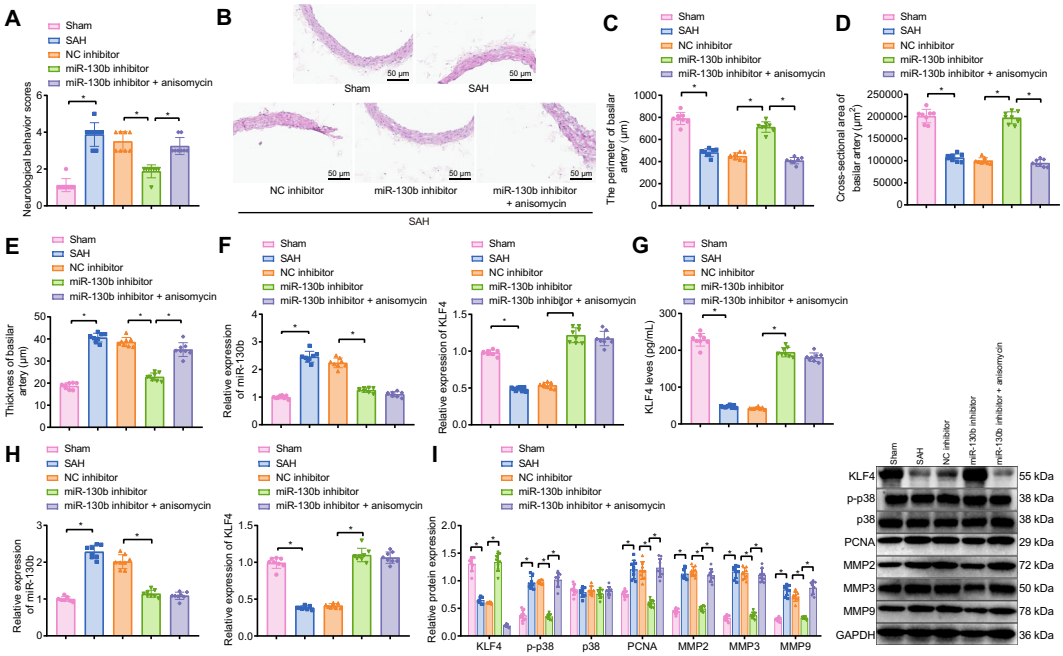

FIG 9 miR-130b promotes CVS following SAH through activation of the p38/MAPK signaling pathway by downregulating *KLF4*. SAH rats were injected with miR-130b inhibitor alone or combined with anisomycin. (A) Neurologic deficit scores after modeling. (B) H&E staining for the cross-section of the basilar artery of SAH rats; (C to E) The semi-quantitative analysis of perimeters of the vascular ring (C), vascular lumen area (D), vascular wall thickness (E) of the cerebral basilar artery in SAH rats by H&E staining. (F) Expression of miR-130b and *KLF4* in CSF in SAH rats detected by RT-qPCR. (G) *KLF4* expression in CSF in SAH rats measured by ELISA. (H) Expression of miR-130b and *KLF4* in the basilar artery in SAH rats detected by RT-qPCR. (I) Expression of *KLF4*, PCNA, MMP2, MMP3, MMP9, p-p38 and p38 in basilar artery of SAH rats detected by Western blot analysis. $^*P < 0.05$. Data between the two groups were compared by paired *t* test. The one-way analysis of variance was used for comparisons among more than two groups, followed by Tukey's post hoc test.

quality of life.[30] Moreover, dysregulated miRNAs with continuous variation of miRNA level in cerebrospinal fluid of SAH patients have been implied in the development of delayed cerebral ischemia, which was perceived as a major contributor to the damaging outcome SAH.[11] In the current research, we investigated the functional role of miR-130b in CVS after SAH through its interaction with its downstream targets. The experimental findings uncovered the tumor-promoting role of miR-130b in CVS following SAH via inhibition of *KLF4* through activation of the p38/MAPK signaling pathway.

First, our results indicated that miR-130b was highly expressed in CVS after SAH and also in SAH rats. Similarly, miRNAs are dysregulated in plasma and CSF in CVS following SAH.[31,32] miR-24 expression has been reported to be increased in SAH patients with vasospasm.[33] In addition, a study has reported that miR-130b-5p expression in peripheral blood is related to the severity of coronary artery disease.[19] Another study has also demonstrated that miR-130b is highly expressed in SAH patients,[11] while the specific mechanisms of miR-130b in CVS after SAH remain unknown. In our study, we first verified that miR-130b was highly expressed in patients with CVS after SAH and in SAH rats.

Meanwhile, the obtained data verified that *KLF4* was a potential target gene of miR-130b in CVS after SAH, and *KLF4* was lowly expressed in CVS following SAH. The functional roles of *KLF4* have been reported in several cardiovascular diseases, including atherosclerosis and thrombosis, as well as in the aortic aneurysm.[34,35] In line with our study, decreased *KLF4* is found in cerebrospinal fluid and plasma of patients with SAH.[25] Furthermore, previous evidence has prompted that *KLF4* regulates the phenotypic modulation of VSMCs in many diseases, including atherosclerosis and cerebral aneurysm.[36]

Besides, we also demonstrated that *KLF4* could inhibit activation of the p38/MAPK signaling pathway, thereby repressing the proliferation and migration of VSMCs. Previous evidence has prompted that KLF4 regulates the phenotypic modulation of VSMCs in many diseases, including atherosclerosis and cerebral aneurysm.[36] Similarly, a recent study has revealed that inhibited *KLF4* transcription aids in the activation of

the p38/MAPK signaling pathway in the event of traumatic brain injury.[37] Nevertheless, another study has indicated that VSMC phenotypic switching is engaged in vascular remodeling and correlated with neurological deficits in SAH.[26] Moreover, mitogen-activated protein kinases are well-known key regulators responsible for transferring the signaling of stress-induced stimuli or extracellular growth factors, exhibiting a critical role in cell regulation processes, such as cell proliferation, migration, and survival.[38,39] Importantly, in the perfusion model experiment, the suppression of the p38 signaling pathway (a member of the MAPK pathway) has been reported to protect neurons.[40]

Further studies concerning CVS in SAH have also manifested that rats with SAH exhibit upregulated p-p38 and p-MAPK expression, whereas activation of p38 and MAPK is closely associated with apoptosis in the cortex.[41] Importantly, the crucial roles of the MAPK signaling pathway in the migration and proliferation of VSMCs have been elaborated in atherosclerosis.[42] Furthermore, a previous study has also demonstrated that the p38/MAPK signaling pathway is activated in CVS, and inhibition of the p38/MAPK signaling pathway suppresses CVS following SAH in rabbits.[43] Therefore, it can be concluded that miR-130b promoted the proliferation and migration of cVSMCs by inhibiting *KLF4* via activation of the p38/MAPK signaling pathway.

In summary, the data presented here demonstrated miR-130b as a major regulator of CVS and its therapeutic significance in SAH. Briefly, in SAH, downregulation of miR-130b expression suppresses the CVS via upregulating *KLF4*, which in turn negatively regulates the p38/MAPK signaling pathway (Fig. 10). In the present study, we identified miRNA as a potential target for the developing therapeutics for SAH; however, further study concerning whether miR-130b/*KLF4* is involved in regulating other SAH symptoms, such as early brain injury, is needed. In addition, whether there are live cells, such as white blood cells, endothelial cells, lymphocytes, and monocyte/macrophages, in the CSF may be the focus of our future work for further validation of the present

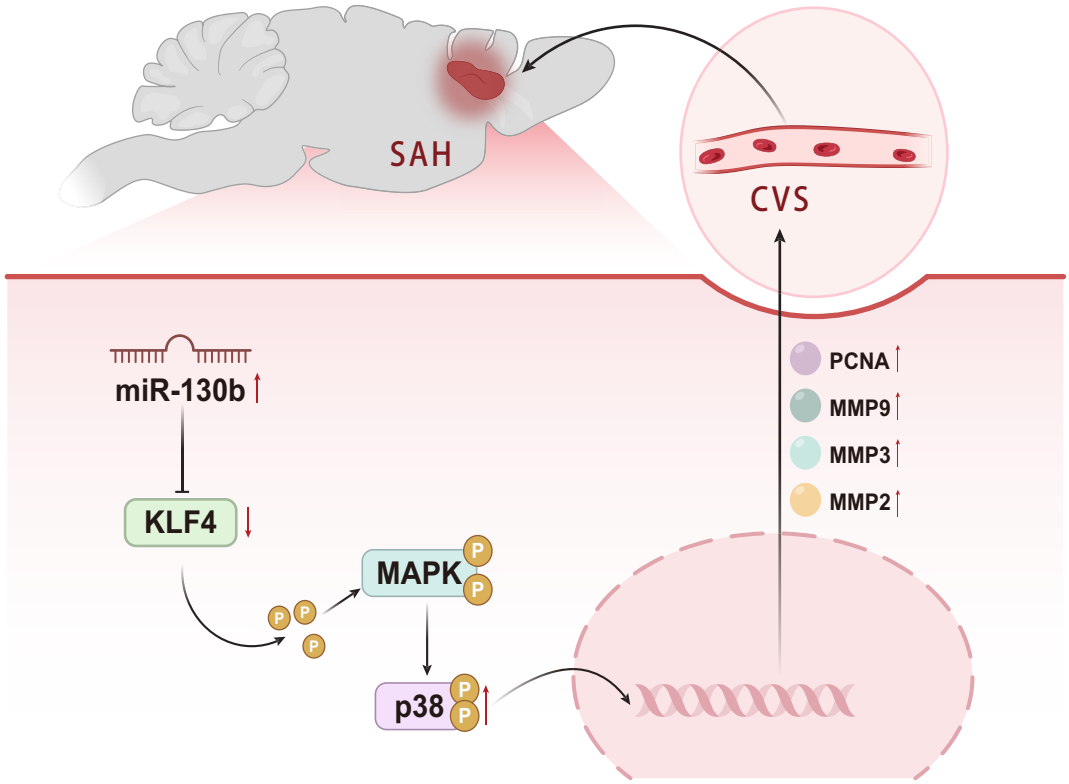

FIG 10 Schematic map of the role of miR-130b-mediated *KLF4* in CVS following SAH. Upregulation of miR-130b induces CVS following SAH by downregulating *KLF4* by activating the p38/MAPK signaling pathway.

findings. Whether *KLF4* might transcriptionally regulate PCNA, MMP2, MMP3, and MMP9 should also be validated.

MATERIALS AND METHODS

Ethical statement. All samples were collected with the informed consent of the patients provided. All research procedures were approved by the ethics committee of Shenzhen People's Hospital by following the Declaration of Helsinki. Animal experiments were implemented according to the principles outlined in the NIH Guide for the Care and Use of Laboratory Animals.

Clinical samples. Our study enrolled 30 patients at our hospital suffering from CVS following SAH and 30 neurologically healthy patients undergoing lower limb surgery (along with spinal anesthesia). Their CSF was collected simultaneously at points 1, 2, 3, 5, and 7 days after surgery. On the first day, a lumbar drainage catheter was placed through the lumbar vertebral interspace into the subarachnoid space of all patients (after intracranial aneurysm rupture), and patients in the control group (after surgery) and external lumbar drainage of CSF was continued for 7 days. The CSF (4 mL) was collected from the lumbar drainage catheter into a 10-mL sterile tube at the same time points on days 1, 2, 3, 5, and 7. After centrifugation (at 12,000 rpm, 4 °C) for 15 min, the supernatant of CSF containing no blood cells was placed into a 1.5 mL centrifuge tube and stored at –80 °C for subsequent experimental detection.

SAH model establishment. Sprague Dawley (SD) adult male rats (weighing 250–300 g) were raised in the standard cage at 23 ± 1 °C under a 12 h light/12 h dark cycle, with free access to food and water. The experiment was conducted after acclimatization for one week.

The SAH was induced by injecting autologous blood into the cisterna magna of adult male SD rats.[41] Briefly, rats were anesthetized via intraperitoneal injection of 3% pentobarbital sodium (30 mg/kg). After that, the middle line of the neck skin was cut longitudinally along the occipital bulge, and the subcutaneous soft tissue was bluntly separated to expose the occipito-occipital membrane fully. Afterward, the cisterna magna was punctured with a syringe, and 0.1 mL of CSF was discarded, followed by the injection of 0.2 mL of autologous blood from arteria femoralis into cisterna magna to induce SAH. In sham-operated rats, normal saline instead of autologous blood was adopted, and the wound was sutured with a medical suture under the aseptic situation to avoid surgical infection.

Subsequently, at 12, 24, 48, and 72 h, respectively, after surgery, eight rats in the sham and SAH groups were taken and anesthetized with 3% pentobarbital by intraperitoneal injection. First, the skin was cut open at the foramen magnum. Next, the muscles were bluntly separated to expose the foramen magnum. Then the meninges were gently pierced with the tip of a 1 mL syringe to extract about 0.1–0.15 mL of colorless to pale yellow CSF into a 1.5 mL centrifuge tube followed by PCR detection of miR-130b and *KLF4* expression and ELISA detection of *KLF4* expression. Rats after CSF collection were euthanized by intraperitoneal injection with three times the amount of anesthetic. Next, the cerebral basilar artery was taken in a 1.5 mL centrifuge tube, stored at –80 °C, and used for RT-qPCR detection of miR-130b and *KLF4* expression. After that, at 12, 24, 48, and 72 h after surgery, eight rats in the sham group and the SAH group, respectively, were taken and anesthetized with 3% pentobarbital by intraperitoneal injection. Next, 60 mL of pre-chilled PBS was perfused with the apex, followed by 60 mL of 4% paraformaldehyde perfusion. Subsequently, the rat cerebral basilar artery was collected for hematoxylin and eosin (H&E) staining of cerebral basilar artery spasm and Western blot analysis for *KLF4*, PCNA, and MMP2, respectively MMP3, MMP9, and p38 protein expression, as well as the expression level of phosphorylated p38.

Animal treatment and grouping. According to the lentivirus transduction instructions, 5 μL negative control (NC) inhibitor lentivirus or miR-130b inhibitor lentivirus (0.1 μM) (Shanghai GenePharma Co. Ltd, Shanghai, China) were mixed with 10 μL co-infective reagent, which was allowed to stand at ambient temperature for 15 min. Anisomycin (HY-18982, MedChemExpress, NJ), a p38/MAPK signaling pathway agonist, was dissolved in dimethylsulfoxide (DMSO) at a concentration of 15 mg/mL. At 24 h before SAH model establishment, 15 μL mixed NC inhibitor solution, 15 μL mixed miR-130b inhibitor solution, and 20 μL Anisomycin solution were injected into the ventricles of SD rats, respectively. Rats were randomized into sham (intraventricular injection of 15 μL normal saline and 20 μL DMSO), SAH (intraventricular injection of 15 μL normal saline and 20 μL DMSO), SAH + NC inhibitor (intraventricular injection of 15 μL mixed NC inhibitor solution and 20 μL DMSO), SAH + miR-130b inhibitor (intraventricular injection of 15 μL mixed miR-130b inhibitor solution and 20 μL DMSO), and SAH + miR-130b inhibitor + anisomycin group (intraventricular injection of 15 μL mixed miR-130b inhibitor solution and 20 μL anisomycin solution).[44]

Behavioral tests for neurological impairment. After SAH modeling, the appetite and activity of the rats in each group were observed before sampling, and the neurobehavioral scores were obtained (details are displayed in Table 1). Then, the three scores were added together to form the neurobehavioral scores of rats, and the mean value and standard deviation of each group of rats were calculated. To ensure the accuracy of the scores, the observer should choose an experimenter who did not know the experimental group.[44]

Reverse transcription quantitative polymerase chain reaction (RT-qPCR). mRNA or miRNA from the patients' CSF or rats' CSF was extracted using a total blood RNA extraction kit (DP433, Tiangen) or a serum miRNA extraction and isolation kit (DP503, Tiangen) based on the instructions. To extract mRNA and miRNA from the cerebral basilar arteries of rats, the TRIzol method was applied according to the reagent specification of the TRIzol kit (16096020 or AM1561, Thermo Fisher Scientific, New York). mRNA was reversely transcribed into cDNA following the instructions of the RT-qPCR kit (ABI). miRNA was reversely transcribed into cDNA in the light of a polyA tailing kit (B53245-0020, Shanghai Bioengineering Co., Ltd, Shanghai, China). The U6 was selected as the internal reference of miR-130b, whereas

TABLE 1 Neurobehavioral scoring scale

		Behavior Score
Appetite	Finished meal	0
	Left meal unfinished	1
	Scarcely ate	2
Activity	Walk and reach at least three corners of the cage	0
	Walk with some stimulation	1
	Almost always lying down	2
Deficits	No deficits	0
	Unstable walk	1
	Impossible to walk	2

TABLE 2 Primer sequences

	Primer sequences
miR-130b (human)	Forward: 5′-CAGTGCAATGATGAAAGGGCAT-3′ Reverse: Universal primer
miR-130b (rat)	Forward: 5′-CAGTGCAATGATGAAAGGGCAT-3′ Reverse: Universal primer
KLF4 (human)	Forward: 5′-CTGCGAACCCACACAGGTG-3′ Reverse: 5′-GGTAGTGCCTGGTCAGTTCATC-3′
KLF4 (rat)	Forward: 5′-CTTTCCTGCCAGACCAGATG-3′ Reverse: 5′-GGTTTCTCGCCTGTGTGAGT-3′
U6 (human, rat)	Forward: 5′-CTCGCTTCGGCAGCACA-3′ Reverse: Universal primer
GAPDH (human)	Forward: 5′-CAACAGCCTCAAGATCATCAGCA-3′ Reverse: 5′-TGGCATGGTCTGTGGTCATGAGT-3′
GAPDH (rat)	Forward: 5′-GCAAGTTCAACGGCACAG-3′ Reverse: 5′-GCCAGTAGACTCCACGACAT-3′

Glyceraldehyde 3-phosphate dehydrogenase (*GAPDH*) was the internal reference of other genes. The relative fold enrichment of target regions was calculated based on the $2^{-\triangle\triangle Ct}$.[45] The used primers are shown in Table 2.

Western blot analysis. Protein extracts were separated and transferred to a polyvinylidene fluoride membrane. First, the primary antibody was added to the membrane for overnight incubation at 37 °C. Then, horseradish peroxidase-labeled secondary antibody (ab205718, goat anti-rabbit or goat anti-mouse, 1:10,000, Abcam) was added for further incubation followed by visualization using enhanced chemiluminescence (Shanghai Baoman Biotechnology, Shanghai, China). The primary antibodies procured from Abcam (CA, UK) included KLF4 (ab215036, 1:1000, rabbit; ab214666, 1:1000, rabbit), α-SMA (ab32575, 1:1000–1:5000, rabbit), PCNA (ab92552, 1:1000–1:10000, rabbit), MMP2 (ab92536, 1:1000–1:5000, rabbit), MMP3 (ab52915, 1:1000–1:20000, rabbit), MMP9 (ab76003, 1:1000–1:20000, rabbit), p-p38 (ab4822, 1:1000, rabbit), p38 (ab170099, 1:1000–1:5000, rabbit). In addition, *GAPDH* (ab181602, 1:10,000, rabbit, Abcam) was used as an internal reference, and the gel image analysis software was used for quantitative analysis.[46]

Enzyme-linked immunosorbent assay (ELISA). The patient's CSF or rat's CSF was diluted 10 times, and then 0.1 mL from each of them was added into a 96-well plate reaction well in the KLF4 ELISA kit (Bio-Swamp, Hubei, China) for incubation at 37 °C for 1 h. The optical density value of each well was measured at 450 nm using an ELISA detector to calculate the *KLF4* concentration.[47]

Isolation of cerebral vascular smooth muscle cells (cVSMCs). SD rats (250–300 g) were anesthetized via intraperitoneal injection of 3% pentobarbital sodium. Under aseptic conditions, the entire brain tissue of the rat was removed and placed in a petri dish containing DMEM/F-12 blank medium (Gibco) supplemented with penicillin-streptomycin. The rat basilar artery was isolated, and the connective tissue and fat around the arterial blood vessels were removed. The blood vessel was cut open, and the inner surface was gently scraped with tweezers to remove the inner membrane of the blood vessel. The blood vessel was then cut into small segments of about 0.2 mm long and treated with 1 mL of a 0.1% collagenase-I solution (Sigma Aldrich) for 30 min under 5% CO_2 until the blood vessels swelled. To further detach the blood vessels, 1 mL of 0.125% trypsin (Gibco) was added for 10 min until the blood vessels became transparent, and then the blood vessels were centrifuged at 1000 rpm for 5 min. Afterward, the precipitated cells were cultured in DMEM/F-12 medium containing 20% FBS. The medium was renewed every three days. After the cell confluence reached 80–90%, trypsinization was performed, followed by cell passage. Cells in passage three were used for experiments. The smooth muscle cell marker protein

α-SMA was labeled with immunofluorescence for cell identification, and cells were cultured in DMEM/F-12 medium containing 10% FBS for the formal experiment.[48]

Cell treatment. cVSMCs were cultured in DMEM/F-12 containing 100 μg/mL streptomycin and 100 U/mL penicillin (Gibco BRL, Grand Island, NY) (37 °C, 5% CO_2, and 95% O_2). Logarithmically growing cells were seeded into six-well plates (3×10^5 cells/well) while platelet-derived growth factor BB (PDGF-BB, 20 ng/mL) was added after 24 h for intervention. After 24 h, cells were further transduced with miR-130b inhibitor or sh-*KLF4* plasmids. After 48 h of transduction, cells were collected for the subsequent experimental procedure.

After PDGF-BB (20 ng/mL) intervention for 24 h, cVSMCs were treated with PDGF-BB and p38/MAPK signaling agonist, i.e., anisomycin, for 24 h and then transfected with NC mimic, miR-130b mimic, overexpression (oe)-NC or oe-*KLF4* plasmids. Following 48 h of transduction, cells were collected for the subsequent experimental procedure.

miRNA targeted luciferase reporter assay. The StarBase, RNAInter, RNA22, miRanda, and mirDIP databases were used to predict the target genes of miR-130b. The five databases use different binding site matching algorithms, and we thus used the Venn tool to perform an intersection analysis of the prediction results from the five databases. The biological prediction website TargetScan algorithm was then applied to verify whether *KLF4* is the direct target gene of miR-130b.

A dual luciferase reporter assay was subsequently used to verify whether *KLF4* was the direct target gene of miR-130b. The cVSMCs at the exponential phase were seeded into six-well plates at a density of 3×10^5 cells/well. Upon reaching 70–80% confluence, cells were cotransfected with correctly synthetic luciferase reporter plasmids *KLF4* WT and MUT with miR-130b mimic, NC mimic, miR-130b inhibitor, and NC inhibitor using the Lipofectamine 3000 reagent (L3000008, Invitrogen). After 48 h, cells were collected, and the luciferase activity was detected by a luciferase detection kit (K801-200, Biovision) through the Lomax20/20 luminometer fluorescence detector (Promega).[49]

H&E staining. The rat brain basilar artery fixed with 4% paraformaldehyde for more than 24 h in different groups was selected, embedded by paraffin, and made into paraffin sections. Then, the sections were stained with hematoxylin for 7 min and then stained with eosin for 1 min.[50] The morphological changes of the vascular ring were observed under an optical microscope, and the perimeter of the vascular ring, the lumen area, and the thickness of the vascular wall was calculated.

Immunofluorescence. After dewaxing and dehydrating, the paraffin sections of the basilar cerebral arteries of rats were subjected to antigen retrieval, blocked with normal goat serum (C-0005, Shanghai Haoran Biotechnology Co., Ltd, Shanghai, China), and immunostained with primary antibodies against KLF4 (ab214666, 1:1000, rabbit, Abcam) and α-SMA (ab32575, 1:500, rabbit, Abcam) at 4 °C overnight. In addition, the sections were incubated with fluorescent secondary antibody (ab150075, 1:200–1:1000, Abcam) for 60 min in the dark and added a fluorescence decay-resistant medium.[50] The fluorescence intensity was observed under a fluorescence microscope.

5-Ethynyl-2′-deoxyuridine (EdU) assay. Cell proliferation was detected by an EdU assay kit (Ribobio, Guangzhou, China) based on the instructions.[51] Images were taken under a fluorescence microscope, and statistical data were collected to record the number of EdU-labeled cells. For example, those whose nuclei were dyed red were labeled positive cells, and the number of positive and negative cells in any three fields was counted under the microscope.

Transwell assay. Transwell chamber (8 mm aperture; Corning) in-vitro cell migration was detected in a 24-well plate.[51] The observation was performed under an inverted fluorescence microscope (TE2000, Nikon, Japan) with five randomly selected fields. The number of cells passing through the chamber was counted, and the average value was taken to be the number of cells passing through the chamber of each group.

Statistics. The results were interpreted using the SPSS 21.0 software (IBM, Armonk, NY). Data between the two groups were compared by paired *t* test. For the comparisons among more than two groups, a one-way analysis of variance was used, followed by Tukey's post hoc test. A comparison of data between groups at different time points by repeated measures analysis of variance followed by Bonferroni correction. Significance criteria were defined as $P < 0.05$.

AUTHORS' CONTRIBUTIONS

Zewei Huang and Jiliang Hu designed the study. Jiongfu Xu and Hao Wang collated the data, and Limeng Dai and Zewei Huang, and Jiliang Hu analyzed and produced the initial draft of the manuscript. Jiongfu Xu and Hao Wang contributed to drafting the manuscript. All authors have read and approved the final submitted manuscript.

FUNDING

This work is supported by Shenzhen Key Laboratory of Prevention and Treatment of Severe Infections [ZDSYS20200811142804014]; Shenzhen Key Medical Discipline Construction Fund [SZXK045]; General project of Shenzhen Nature Fund [JCYJ20210324114008023]; Special [2022N070] Research, development and application of low-injury interventional embolization system for ischemic stroke.

ORCID

Hao Wang http://orcid.org/0000-0002-2386-5870

DATA AVAILABILITY STATEMENT

The data that supports the findings of this study are available at https://doi.org/10.6084/m9.figshare.22707802.

REFERENCES

1. Long B, Koyfman A, Runyon MS. Subarachnoid hemorrhage: updates in diagnosis and management. Emerg Med Clin North Am. 2017;35:803–824. doi:10.1016/j.emc.2017.07.001.
2. Boling B, Groves TR. Management of subarachnoid hemorrhage. Crit Care Nurse. 2019;39:58–67. doi:10.4037/ccn2019882.
3. Ogunlaja OI, Cowan R. Subarachnoid hemorrhage and headache. Curr Pain Headache Rep. 2019;23:44. doi:10.1007/s11916-019-0785-x.
4. Abraham MK, Chang WW. Subarachnoid hemorrhage. Emerg Med Clin North Am. 2016;34:901–916. doi:10.1016/j.emc.2016.06.011.
5. Sundstrom J, Soderholm M, Soderberg S, Alfredsson L, Andersson M, Bellocco R, Bjorck M, Broberg P, Eriksson M, Eriksson M, et al. Risk factors for subarachnoid haemorrhage: a nationwide cohort of 950 000 adults. Int J Epidemiol. 2019;48:2018–2025. doi:10.1093/ije/dyz163.
6. Andersen CR, Presseau J, Saigle V, Etminan N, Vergouwen MDI, English SW. Core outcomes for subarachnoid haemorrhage. Lancet Neurol. 2019;18:1075–1076. doi:10.1016/S1474-4422(19)30412-0.
7. Cortez MA, Bueso-Ramos C, Ferdin J, Lopez-Berestein G, Sood AK, Calin GA. MicroRNAs in body fluids–the mix of hormones and biomarkers. Nat Rev Clin Oncol. 2011;8:467–477. doi:10.1038/nrclinonc.2011.76.
8. Song MA, Paradis AN, Gay MS, Shin J, Zhang L. Differential expression of microRNAs in ischemic heart disease. Drug Discov Today. 2015;20:223–235. doi:10.1016/j.drudis.2014.10.004.
9. Tutar Y. miRNA and cancer; computational and experimental approaches. Curr Pharm Biotechnol. 2014;15:429. doi:10.2174/1389201015051408281 61335.
10. Ziats MN, Rennert OM. Identification of differentially expressed microRNAs across the developing human brain. Mol Psychiatry. 2014;19:848–852. doi:10.1038/mp.2013.93.
11. Bache S, Rasmussen R, Rossing M, Laigaard FP, Nielsen FC, Moller K. MicroRNA changes in cerebrospinal fluid after subarachnoid hemorrhage. Stroke. 2017;48:2391–2398. doi:10.1161/STROKEAHA.117.017804.
12. Lopes KP, Vinasco-Sandoval T, Vialle RA, Paschoal FM, Jr., Bastos V, Bor-Seng-Shu E, Teixeira MJ, Yamada ES, Pinto P, Vidal AF, et al. Global miRNA expression profile reveals novel molecular players in aneurysmal subarachnoid haemorrhage. Sci Rep. 2018;8:8786. doi:10.1038/s41598-018-27078-w.
13. Gu JJ, Fan KC, Zhang JH, Chen HJ, Wang SS. Suppression of microRNA-130b inhibits glioma cell proliferation and invasion, and induces apoptosis by PTEN/AKT signaling. Int J Mol Med. 2018;41:284–292.
14. Lei Y, Yang M, Li H, Xu R, Liu J. miR-130b regulates PTEN to activate the PI3K/Akt signaling pathway and attenuate oxidative stress-induced injury in diabetic encephalopathy. Int J Mol Med. 2021;48:141. doi:10.3892/ijmm.2021.4974.
15. Zhang H, Li D, Zhang Y, Li J, Ma S, Zhang J, Xiong Y, Wang W, Li N, Xia L. Knockdown of lncRNA BDNF-AS suppresses neuronal cell apoptosis via downregulating miR-130b-5p target gene PRDM5 in acute spinal cord injury. RNA Biol. 2018;15:1071–1080. doi:10.1080/15476286.2018.1493333.
16. Hirono T, Jingushi K, Nagata T, Sato M, Minami K, Aoki M, Takeda AH, Umehara T, Egawa H, Nakatsuji Y, et al. MicroRNA-130b functions as an oncomiRNA in non-small cell lung cancer by targeting tissue inhibitor of metalloproteinase-2. Sci Rep. 2019;9:6956. doi:10.1038/s41598-019-43355-8.
17. Yu T, Cao R, Li S, Fu M, Ren L, Chen W, Zhu H, Zhan Q, Shi R. MiR-130b plays an oncogenic role by repressing PTEN expression in esophageal squamous cell carcinoma cells. BMC Cancer. 2015;15:29. doi:10.1186/s12885-015-1031-5.
18. Zhang Q, Zhang B, Sun L, Yan Q, Zhang Y, Zhang Z, Su Y, Wang C. MicroRNA-130b targets PTEN to induce resistance to cisplatin in lung cancer cells by activating Wnt/beta-catenin pathway. Cell Biochem Funct. 2018;36:194–202. doi:10.1002/cbf.3331.
19. Coban N, Ozuynuk AS, Erkan AF, Guclu-Geyik F, Ekici B. Levels of miR-130b-5p in peripheral blood are associated with severity of coronary artery disease. Mol Biol Rep. 2021;48:7719–7732. doi:10.1007/s11033-021-06780-5.
20. Liu ZD, Wang Q, Pan DQ, Meng FQ, Li JT, Wang YH. MicroRNA-130b inhibits cerebral ischemia/reperfusion induced cell apoptosis via regulation of IRF1. Eur Rev Med Pharmacol Sci. 2020;24:12334–12341.
21. Zheng Y, Wang L, Chen M, Pei A, Xie L, Zhu S. Upregulation of miR-130b protects against cerebral ischemic injury by targeting water channel protein aquaporin 4 (AQP4). Am J Transl Res. 2017;9:3452–3461.
22. Cowan CE, Kohler EE, Dugan TA, Mirza MK, Malik AB, Wary KK. Kruppel-like factor-4 transcriptionally regulates VE-cadherin expression and endothelial barrier function. Circ Res. 2010;107:959–966. doi:10.1161/CIRCRESAHA.110.219592.
23. Hale AT, Tian H, Anih E, Recio FO, 3rd, Shatat MA, Johnson T, Liao X, Ramirez-Bergeron DL, Proweller A, Ishikawa M, et al. Endothelial Kruppel-like factor 4 regulates angiogenesis and the Notch signaling pathway. J Biol Chem. 2014;289:12016–12028. doi:10.1074/jbc.M113.530956.
24. Shatat MA, Tian H, Zhang R, Tandon G, Hale A, Fritz JS, Zhou G, Martinez-Gonzalez J, Rodriguez C, Champion HC, et al. Endothelial Kruppel-like factor 4 modulates pulmonary arterial hypertension. Am J Respir Cell Mol Biol. 2014;50:647–653. doi:10.1165/rcmb.2013-0135OC.
25. Kikkawa Y, Ogura T, Nakajima H, Ikeda T, Takeda R, Neki H, Kohyama S, Yamane F, Kurogi R, Amano T, et al. Altered expression of microRNA-15a and Kruppel-like factor 4 in cerebrospinal fluid and plasma after aneurysmal subarachnoid hemorrhage. World Neurosurg. 2017;108:909–916.e903. doi:10.1016/j.wneu.2017.09.008.
26. Wang L, Zhang Z, Liang L, Wu Y, Zhong J, Sun X. Anti-high mobility group box-1 antibody attenuated vascular smooth muscle cell phenotypic switching and vascular remodelling after subarachnoid haemorrhage in rats. Neurosci Lett. 2019;708:134338. doi:10.1016/j.neulet.2019.134338.
27. Jia Y, Zhou J, Luo X, Chen M, Chen Y, Wang J, Xiong H, Ying X, Hu W, Zhao W, et al. KLF4 overcomes tamoxifen resistance by suppressing MAPK signaling pathway and predicts good prognosis in breast cancer. Cell Signal. 2018;42:165–175. doi:10.1016/j.cellsig.2017.09.025.
28. Guo Z, Hu Q, Xu L, Guo ZN, Ou Y, He Y, Yin C, Sun X, Tang J, Zhang JH. Lipoxin A4 reduces inflammation through formyl peptide receptor 2/p38 MAPK signaling pathway in subarachnoid hemorrhage rats. Stroke. 2016;47:490–497. doi:10.1161/STROKEAHA.115.011223.
29. Park HS, Quan KT, Han JH, Jung SH, Lee DH, Jo E, Lim TW, Heo KS, Na M, Myung CS. Rubiarbonone C inhibits platelet-derived growth factor-induced proliferation and migration of vascular smooth muscle cells through the focal adhesion kinase, MAPK and STAT3 Tyr(705) signalling pathways. Br J Pharmacol. 2017;174:4140–4154. doi:10.1111/bph.13986.
30. Lu G, Wong MS, Xiong MZQ, Leung CK, Su XW, Zhou JY, Poon WS, Zheng VZY, Chan WY, Wong GKC. Circulating microRNAs in delayed cerebral infarction after aneurysmal subarachnoid hemorrhage. J Am Heart Assoc. 2017;6:e005363.
31. Chan MTH, Wong JYY, Leung AKT, Lu G, Poon WS, Lau AY, Chan WY, Wong GKC. Plasma and CSF miRNA dysregulations in subarachnoid hemorrhage reveal clinical courses and underlying pathways. J Clin Neurosci. 2019;62:155–161. doi:10.1016/j.jocn.2018.11.038.
32. Wang WX, Springer JE, Xie K, Fardo DW, Hatton KW. A highly predictive microRNA panel for determining delayed cerebral vasospasm risk following aneurysmal subarachnoid hemorrhage. Front Mol Biosci. 2021;8:657258. doi:10.3389/fmolb.2021.657258.
33. Li HT, Wang J, Li SF, Cheng L, Tang WZ, Feng YG. Upregulation of microRNA-24 causes vasospasm following subarachnoid hemorrhage by suppressing the expression of endothelial nitric oxide synthase. Mol Med Rep. 2018;18:1181–1187.
34. Salmon M, Johnston WF, Woo A, Pope NH, Su G, Upchurch GR, Jr., Owens GK, Ailawadi G. KLF4 regulates abdominal aortic aneurysm morphology and deletion attenuates aneurysm formation. Circulation. 2013;128:S163–S174. doi:10.1161/CIRCULATIONAHA.112.000238.

35. Zhou G, Hamik A, Nayak L, Tian H, Shi H, Lu Y, Sharma N, Liao X, Hale A, Boerboom L, et al. Endothelial Kruppel-like factor 4 protects against atherothrombosis in mice. J Clin Invest. 2012;122:4727–4731. doi:10.1172/JCI66056.
36. Zeng Q, Wei B, Zhao Y, Wang X, Fu Q, Liu H, Li F. Shh mediates PDGF-induced contractile-to-synthetic phenotypic modulation in vascular smooth muscle cells through regulation of KLF4. Exp Cell Res. 2016;345:82–92. doi:10.1016/j.yexcr.2016.05.014.
37. Wang Z, Li J, Wang A, Wang Z, Wang J, Yuan J, Wei X, Xing F, Zhang W, Xing N. Sevoflurane inhibits traumatic brain injury-induced neuron apoptosis via EZH2-downregulated KLF4/p38 axis. Front Cell Dev Biol. 2021;9:658720. doi:10.3389/fcell.2021.658720.
38. Kim EK, Choi EJ. Pathological roles of MAPK signaling pathways in human diseases. Biochim Biophys Acta. 2010;1802:396–405. doi:10.1016/j.bbadis.2009.12.009.
39. Kim EK, Choi EJ. Compromised MAPK signaling in human diseases: an update. Arch Toxicol. 2015;89:867–882. doi:10.1007/s00204-015-1472-2.
40. Liao W, Zhong Y, Cheng W, Dong LF. 3-N-butylphthalide inhibits neuronal apoptosis in rats with cerebral infarction via targeting P38/MAPK. Eur Rev Med Pharmacol Sci. 2019;23:144–152.
41. Huang Q, Wang G, Hu YL, Liu JX, Yang J, Wang S, Zhang HB. Study on the expression and mechanism of inflammatory factors in the brain of rats with cerebral vasospasm. Eur Rev Med Pharmacol Sci. 2017;21:2887–2894.
42. Li W, Zhi W, Liu F, Zhao J, Yao Q, Niu X. Paeoniflorin inhibits VSMCs proliferation and migration by arresting cell cycle and activating HO-1 through MAPKs and NF-kappaB pathway. Int Immunopharmacol. 2018;54:103–111. doi:10.1016/j.intimp.2017.10.017.
43. Zhang X, Zhao XD, Shi JX, Yin HX. Inhibition of the p38 mitogen-activated protein kinase (MAPK) pathway attenuates cerebral vasospasm following experimental subarachnoid hemorrhage in rabbits. Ann Clin Lab Sci. 2011;41:244–250.
44. Yuan S, Yu Z, Zhang Z, Zhang J, Zhang P, Li X, Li H, Shen H, Chen G. RIP3 participates in early brain injury after experimental subarachnoid hemorrhage in rats by inducing necroptosis. Neurobiol Dis. 2019;129:144–158. doi:10.1016/j.nbd.2019.05.004.
45. Lai N, Wu D, Liang T, Pan P, Yuan G, Li X, Li H, Shen H, Wang Z, Chen G. Systemic exosomal miR-193b-3p delivery attenuates neuroinflammation in early brain injury after subarachnoid hemorrhage in mice. J Neuroinflammation. 2020;17:74. doi:10.1186/s12974-020-01745-0.
46. Xu G, Guo J, Sun C. Eucalyptol ameliorates early brain injury after subarachnoid haemorrhage via antioxidant and anti-inflammatory effects in a rat model. Pharm Biol. 2021;59:114–120.
47. Liu L, Zhang P, Zhang Z, Hu Q, He J, Liu H, Zhao J, Liang Y, He Z, Li X, et al. LXA4 ameliorates cerebrovascular endothelial dysfunction by reducing acute inflammation after subarachnoid hemorrhage in rats. Neuroscience. 2019;408:105–114. doi:10.1016/j.neuroscience.2019.03.038.
48. Dang B, Shen H, Li H, Zhu M, Guo C, He W. Matrix metalloproteinase 9 may be involved in contraction of vascular smooth muscle cells in an in vitro rat model of subarachnoid hemorrhage. Mol Med Rep. 2016;14:4279–4284. doi:10.3892/mmr.2016.5736.
49. Kim JW, Jang SM, Kim CH, An JH, Kang EJ, Choi KH. New molecular bridge between RelA/p65 and NF-kappaB target genes via histone acetyltransferase TIP60 cofactor. J Biol Chem. 2012;287:7780–7791. doi:10.1074/jbc.M111.278465.
50. Qiu J, Li W, Mu R, Wang L, Guo L, Ma L. MFGE8 decreased neuronal apoptosis and neuroinflammation to ameliorate early brain injury induced by subarachnoid hemorrhage through the inhibition of HMGB1. Hum Exp Toxicol. 2022;41:9603271221093635. doi:10.1177/09603271221093635.
51. Zhu J, Liu B, Wang Z, Wang D, Ni H, Zhang L, Wang Y. Exosomes from nicotine-stimulated macrophages accelerate atherosclerosis through miR-21-3p/PTEN-mediated VSMC migration and proliferation. Theranostics. 2019;9:6901–6919. doi:10.7150/thno.37357.